JTTEE5 16:220–228
DOI: 10.1007/s11666-007-9034-7
1059-9630/$19.00 © ASM International

Peer Reviewed

Effect of Heat Treatments on HVOF Hydroxyapatite Coatings

J. Fernández, M. Gaona, and J.M. Guilemany

(Submitted September 13, 2006; in revised form February 19, 2007)

Highly crystalline hydroxyapatite (HAp) powder was thermally sprayed onto Ti-6Al-4V substrates using the High-Velocity Oxy-Fuel (HVOF) process. Coatings were heat treated for 60 min at 700 °C to study the influence of the crystallization on chemical and mechanical properties. Characterization of the HAp coatings was carried out by Fourier Transform Infrared Spectroscopy (FTIR) and x-ray diffraction (XRD) using Rietveld analysis. The results showed that the coatings were highly crystalline (82%) and no other phases of calcium phosphate were present. Coatings were 100% crystalline after the heat treatment. Bioactivity of the coatings was investigated by immersion in Kokubo's simulated body fluid. The dissolution/precipitation behavior was studied and the degradation of HAp coatings caused by the immersion test was studied by measuring the adhesion strength of the coatings. After immersion in SBF bond strength decreased for the as-sprayed coatings, without any thermal treatment, but it was constant for the heat-treated coatings. This phenomenon was related to the dissolution of the amorphous phase in the interface substrate-coating in the as-sprayed coatings.

Keywords adhesion test, heat treatment, high-velocity oxy-fuel spraying, hydroxyapatite, immersion test

1. Introduction

Hydroxyapatite is chemically similar to the mineral component of bones and hard tissues in mammals (Ref 1). It is one of the few materials that are considered bioactive, meaning that it will support bone in growth and Osseo integration when used in orthopedic, dental, and maxillofacial applications. Moreover, HAp has the capacity of creating a stable adhesion with the adjacent bone and does not generate pathological reaction or low inflammatory cell response, when used as orthopedic implant.

In spite of HAp's excellent properties as biomaterial, its inherent mechanical properties (brittleness, low fracture toughness) have restricted its use in many load-bearing applications (Ref 2, 3). Metallic implants are currently being used as load-bearing implants, and polymer, ceramic, or composite implants are typically used as non-load-bearing implants or as coatings (Ref 4). HAp coatings for total joint implants were introduced in the mid-1980s to improve fixation between bone and implant (Ref 5, 6). Several techniques can be used to deposit HAp coatings as dip coating-sintering (Ref 7, 8), hot isostatic pressing (HIP) (Ref 9), electrophoretic deposition (Ref 10), ion-beam sputtering coating (Ref 11, 12), biomimetic deposition (Ref 13, 14) but commercially, the most commonly used are thermal spray techniques such as Atmospheric Plasma Spraying (APS) (Ref 15), Vacuum Plasma Spraying (VPS) (Ref 16) and High-Velocity Oxy-Fuel spraying (HVOF) (Ref 17).

Thermal spray techniques involve partial melting of the HAp powder and its acceleration toward a substrate. Sprayed material solidifies rapidly on impacting onto the substrate producing the coating. Plasma spray is one of the most used techniques due to numerous advantages such as simplicity, high deposition rates, low substrate temperature, variable coating porosity, phases, and structure. The main problem in plasma-sprayed HAp coatings is the generation of amorphous calcium phosphate (ACP) and bioactive calcium phosphate phase such as tetra calcium phosphate (TTCP), tricalcium phosphate (TCP), metastable crystalline products such as oxyhydroxyapatite (OHAp, $Ca_{10}(PO_4)_6(OH)_{2-2x}O_x\theta_x$) or oxyapatite (OAp, $Ca_{10}(PO_4)_6O_2$) and the formation of CaO (Ref 18, 19). The presence of large amounts of ACP is undesirable since its strong in vivo resorption may cause mechanical and adhesive instabilities of the coating. Degradation of HAp coatings with high amorphous phase content occurs by delamination of cracked lamellae and dissolution of the remaining lamellae during immersion tests (Ref 20).

As an alternative, HVOF is a rather new technique to obtain HAp coatings onto metallic substrates. The HVOF thermal spraying process is based on the principle of a combustion of fuel and oxygen gases in a chamber. Fuel gases used are hydrogen, propylene, propane, or acetylene. The combination of high gas flow rates and high pressure in the combustion chamber leads the generation of a supersonic flame which reaches a speed of 2000 m s^{-1} and the particle speed may reach 800 m s^{-1} (Ref 21). This technique has the same advantages of Atmospheric

J. Fernández, M. Gaona, and **J.M. Guilemany,** CPT Thermal Spray Centre, Materials Engineering, Dept. de Ciència dels Materials i Enginyeria Metallúrgica, Universitat de Barcelona, C/Martí i Franquès, 1, 08028, Barcelona, Spain. Contact e-mail: cpt-cmem@ub.edu.

Plasma Spray, but the use of a cooler and faster flame allows obtaining HAp coatings without the lack of crystallinity of APS. However, HVOF as-sprayed coating is not 100% crystalline. Some authors have demonstrated that in the presence of hydrostatic pressure or water vapor, an appropriate heat treatment, could promote the crystallization of ACP to HAp (Ref 22-25). The objective of this work was to obtain HAp coatings by means of HVOF and to study the influence of crystallization, on heat treatment, on the properties of the coatings.

2. Materials and Methods

HAp powder used was from Plasma Biotal Ltd. (UK). Particle size distribution was determined by a HVOF LS 13320 Laser Diffraction Particle Analyser (Beckman Coulter, Inc., Fullerton, CA, EEUU). Coatings were deposited on previously grit blasted Ti-6Al-4V substrates with a DJH 2600 HVOF system (Sulzer Metco, Inc., Westbury, NY). Used spraying parameters were selected according to previous experiments. Hydrogen was the fuel gas and the powder carrier gas was nitrogen. The flow rates were 180-200 SLPM for oxygen and 600-650 SLPM for hydrogen. Spray distance was 225 mm and a powder feed-rate of 30-40 g/min was used.

Heat treatment was carried out in air, in a high-temperature furnace, in order to reduce or eliminate the ACP content. The amorphous-crystalline phase transformation was reported to occur from 500 to 700 °C (Ref 26, 27). The as-sprayed coatings were heat treated at 700 °C for 1 h. Then the samples were slowly cooled down to room temperature inside the furnace. The Ti-6Al-4V β-transus temperature is 980 °C (Ref 28), so the substrate maintains a mill-annealed structure.

Samples were cut with a diamond cut-off wheel and ultrasound cleaned in acetone for 10 min. Then the coatings were cold mounted with epoxy resin under vacuum impregnation. As-sprayed surface and cross-sectional morphology of coatings were characterized with a Scanning Electron Microscope (JEOL 5310, Tokyo, Japan). Ten images of the cross section of each coating were analyzed via image analysis to determine the porosity levels. The ratio of calcium to phosphorus (Ca/P) in the coatings was measured using a Röntec Energy Dispersive Spectroscopy Analyser (Bruker AXS Microanalysis GmbH, Berlin, Germany) coupled to the SEM. Coatings were etched with an acidic solution (2% HNO_3) after the sample was embedded with the epoxy resin to remove the amorphous phase of the coating.

Qualitative phase composition of the starting powder and the as-sprayed coatings were analyzed by x-ray diffractometer SIEMENS D500 (Cu Kα1 + 2, 40 kV, 30 mA). Quantitative phase composition analysis was carried out using the Rietveld method, with the Winproof program. Subsequently, this analysis was performed to determine the degree of crystallinity of the coatings. The analysis multiplies the function for each reflection in the x-ray powder diffraction pattern, which can simulate the shape of the reflection peak to integrate intensity of the obtained from the structure model, and then refine the function parameters to fit the measured reflection intensity (Ref 29). To run the analysis it was therefore necessary to remove the substrate and mix the ''coating'' with ZnO as a standard for the Rietveld analysis. The mixture was then analyzed with a Siemens θ/2θ D-500 diffractometer in Bragg-Brentano geometry. Cu Kα radiation was used ($\lambda = 1.5418$ Å) with a graphite monochromator. Data from 8 to 80° (2θ) were collected with a step size of 0.02° and a counting time of 24 s. Structural investigation of the coating and the powder was carried out using DA3 Fourier transform spectrometer (ABB Bomem, Inc., Zurich, Switzerland). Spectra were recorded from a KBr pellet over 4000-400 cm^{-1}. The spectrum of the HAp was then compared with the literature. Average roughness (R_a) was measured using a Surftest 301 roughness tester (Mitutoyo, Tokyo, Japan). R_a is the average deviation of the profile from a mean line.

Coated samples were immersed in Simulated Body Fluid (SBF) between 1 and 7 days. SBF was prepared in accordance to Kokubo (Ref 30), and pH was adjusted at 7.4 at 36.5 °C with tris (hydroxymethylaminomethane) and hydrochloric acid. The final inorganic ion concentration (in mm/L) was 142.0 Na^+, 5.0 K^+, 1.5 Mg^{2+}, 2.5 Ca^{2+}, 148.8 Cl^-, 4.2 HCO^{3-}, 1.0 HPO_4^{2-}, and 0.5 SO_4^{2-}. After immersion, samples were rinsed with distilled water and dried in air. Free-surface coated samples were observed by SEM, and the solutions were analyzed using Elan-6000 Inductively Coupled Plasma-Atomic Emission (ICP-AE) Spectrophotometer (Perkin-Elmer, USA). The concentration of Ca^{2+} and HPO_4^{2-} were determined as a function of the different immersion times. An average of three measures for every immersion time was used.

Bond Strength was measured after immersion in SBF using tensile test ASTM F1147-99 which is especially designed for plasma-sprayed HAp coatings (Ref 31). Fracture surfaces were observed using binocular lens with Image Analysis to determine what type of failure mechanism took place (cohesive, adhesive, or through the glue).

3. Results

3.1 HAp Feedstock Powder

Scanning Electron Microscope micrographs reveal the irregular morphology of the sintered and crushed particles. Mean size was 32.59 ± 3.08 μm. XRD patterns were recorded and compared with HAp JCPDS 9-432 card (Ref 32). Structural parameters of the feedstock powder were calculated using the Rietveld analysis. Unit cell dimensions of feedstock powder were $a = 0.9413$ nm and $c = 0.6884$ nm. Many investigations of such crystals have been carried out using x-ray diffraction analysis achieving similar results (Ref 33, 34).

Figure 1, curve (a) shows the Fourier Transform Infrared (FTIR) spectrum of the feedstock powder that exhibits the stretching (3572 cm^{-1}) and the hindered

rotation mode of the hydroxyl group (633 cm^{-1}). The broad band about 3430 cm^{-1} is attributed of adsorbed molecules of water on the surface. The peaks at 1092, 1047, and 948 cm^{-1} represent the stretching vibration mode of PO_4^{3-} characteristic for HAp and the bands at 566 and 603 cm^{-1} are assigned as the bending mode (Table 1) (Ref 35). The peaks appearing at 2000-2500 cm^{-1} are carbonate peaks resulting from the absorption of carbon dioxide from the atmosphere.

3.2 Phase Analysis using XRD

Figure 2 shows XRD pattern of the HAp starting powder (a), as well as the as-sprayed (b), and the heat-treated HAp coatings (c). The peaks are broader in the as-sprayed coating pattern than in the heat-treated ones and a slight ''hump'' centered about $2\theta = 30\text{-}35°$ elevated from the background attests to the presence of ACP in the as-sprayed coating. This hump disappears after the heat treatment at 700 °C for 1 h (Fig. 2(c)). Consequently, HAp was the only crystalline phase present in the coatings. No other crystalline calcium phosphate phases were found in the coating as a result of the thermal decomposition of HAp during the coating deposition (Ref 36). Experimental and calculated XRD patterns show a very good Rietveld fit ($\chi^2 = 2.79$). It was found that the content of crystalline HAp was 82 and 18% of ACP, in the as-sprayed coating, and no evidence of ACP in the heat-treated coating was found.

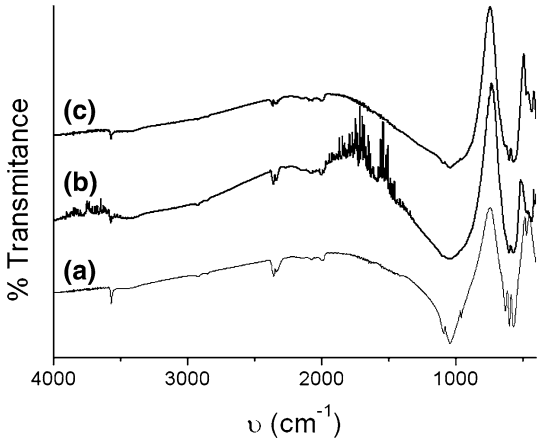

Fig. 1 FTIR of (a) HAp feedstock powder, (b) as-sprayed HAp coatings, and (c) heat-treated coatings (700 °C, 1 h)

Table 1 Observed infrared band positions for HAp feedstock powder and both coatings

Peak assignments	HAp powder	As-sprayed coating	Postheat treatment
Hydroxyl stretch $\nu_{s,OH}$	3572	3572	3572
Phosphate ν_3 (f_2)	1092	1097	1090
	1047	1038	1048
	–	–	–
Phosphate ν_1 (a)	948	958	960
Hydroxyl $\nu_{1,\ OH}$	633	–	630
Phosphate ν_4 (f_2)	603	602	601
	566	567	570

3.3 Microstructural Characterization

Figure 3 shows the representative surface morphology of a HVOF hydroxyapatite coating. The irregular free

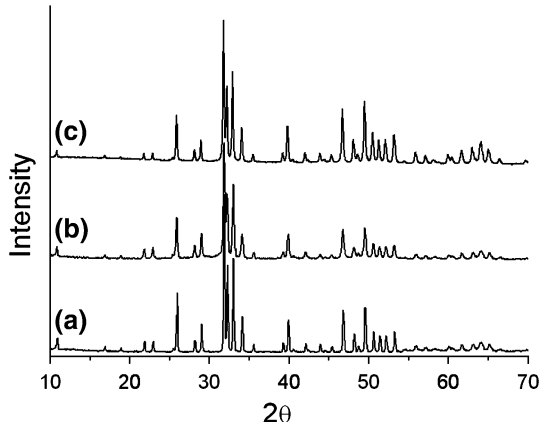

Fig. 2 X ray diffraction (XRD) pattern of (a) the HAp feedstock powder, (b) as-sprayed HAp coatings, and (c) heat-treated HAp coatings (700 °C, 1 h). All the peaks can be assigned to HAp

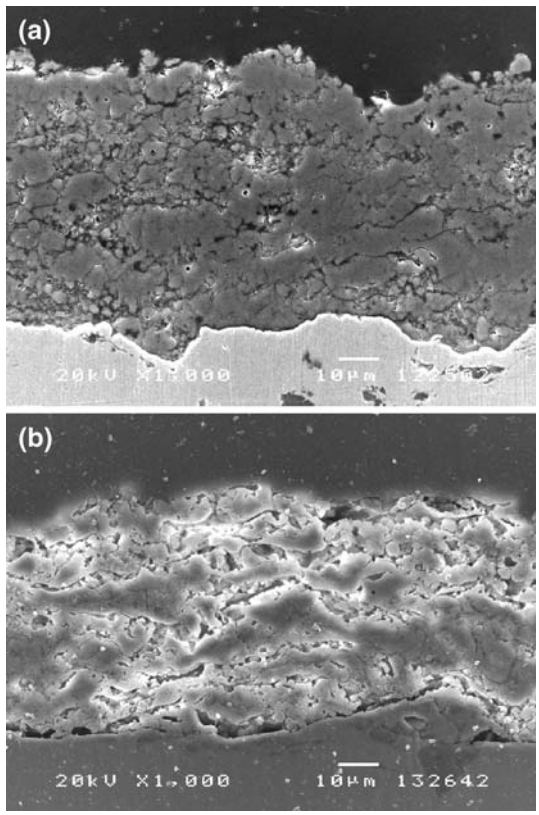

Fig. 3 (a) Polished cross section of the as-sprayed coating. (b) Etched polished cross section of the as-sprayed coating

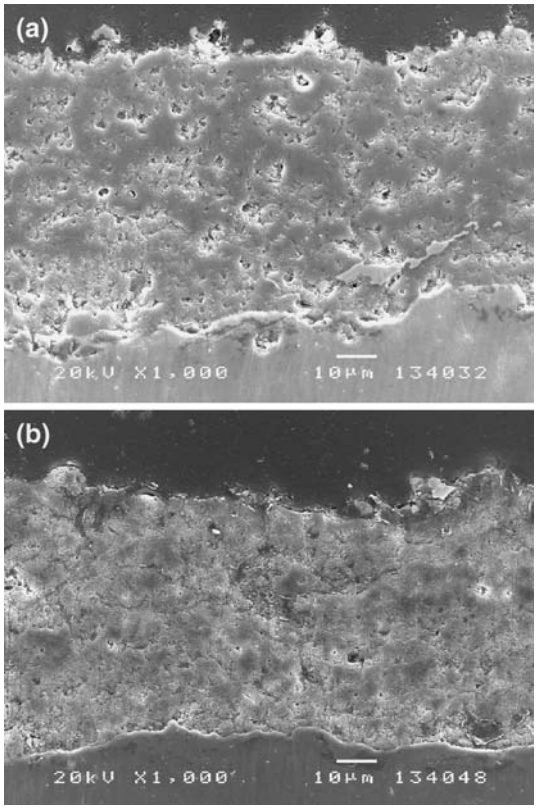

Fig. 4 (a) Polished cross section of the heat-treated coating. (b) Etched polished cross section of the heat-treated coating

surface of the as-sprayed coating is clearly seen. The as-sprayed coating was composed of tightly adhered splats. Well-flattened splats with smooth glassy appearance and irregular regions are distinguished. Glassy regions are considered to be ACP and the irregular regions are formed by residual crystallites from the high crystalline powder and agglomerated splat debris (Ref 37). No visible differences in surface morphologies were observed between as-sprayed and heat-treated coatings (Fig. 3 and 4).

Polished cross sections of as-sprayed HVOF hydroxyapatite and of the heat-treated coatings are shown in Fig. 3 and 4, respectively. There is no evidence of cracking in both coatings. Heat treatment results in a decrease of the porosity of the as-sprayed coating. Figure 3(b) and 4(b) show the coatings after etching by a solution of HNO_3 (2%). Chemical etching preferentially removes the amorphous phase of the coating and let the lamellar structure stand out (Fig. 3(b)). Amorphous phase appears at the interface of every lamella, parallel to the substrate-coating interface and at the interface coating-substrate. Furthermore, on etched heat-treated coatings no removal of material was observed so confirming that no amorphous phase was present (Fig. 4(b)), which is in the agreement with the XRD Rietveld fit.

A total of 15 measurements for thickness, roughness, and porosity were carried out for each coating. Thickness of the as-sprayed coatings was 68.6 ± 6.0 μm and the surface roughness was 4.2 ± 0.4 μm. After heat treatment the cross-sectional thickness was measured to be 67.6 ± 5.4 μm and the coating roughness was 4.1 ± 0.7 μm. The thickness and the roughness are similar for both coatings, so these parameters are not affected by the heat treatment. However a change in porosity can be deduced from the SEM images between as-sprayed and crystallized coatings. The porosity of the as-sprayed coatings was $13 \pm 2\%$, whereas for the annealed coating was $6 \pm 1\%$.

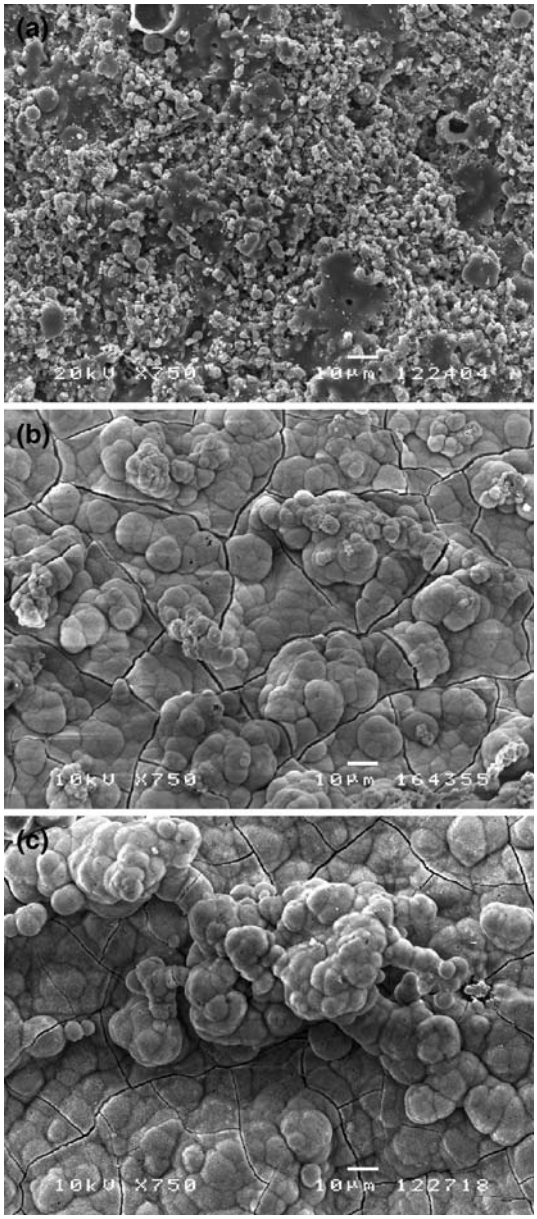

Fig. 5 As-sprayed coating after immersion test. (a) 0 days, (b) 7 days, and (c) 14 days

3.4 Elemental Analysis using EDS

Elemental identification by EDS was used to provide information about the Ca/P ratio. It was found that the

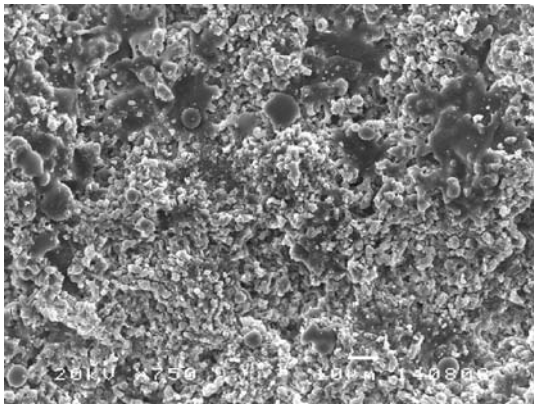

Fig. 6 Heat-treated coating after 14 days of immersion

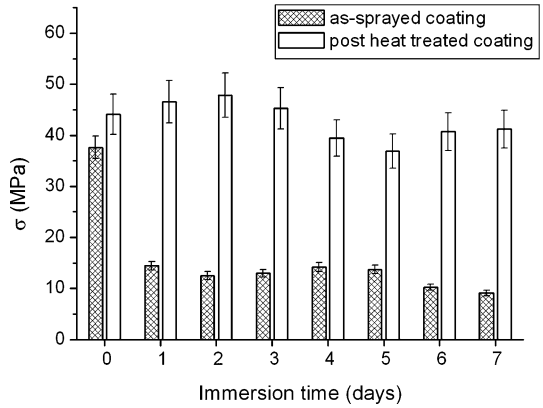

Fig. 8 Adhesion test results according to ASTM F1147-99

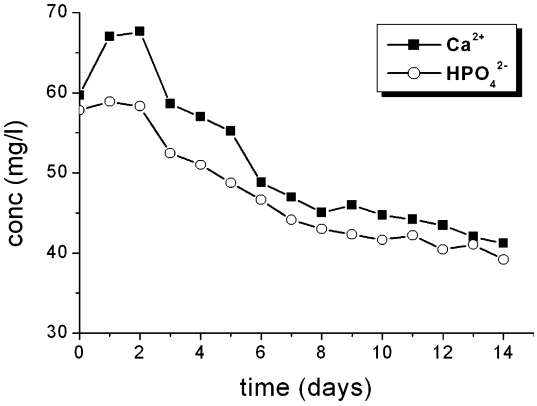

Fig. 7 Evolution of the concentration of Ca^{2+} and HPO_4^{2-} in SBF during immersion test

relations Ca/P were 1.70 for the HVOF as-sprayed coating, and 1.68 for the heat-treated coating, very close to the relation of the feedstock HAp powder, 1.67.

3.5 Structural Analysis using FTIR

Due to the close to identical structure of HAp and oxy- and oxyhydroxyapatite (OAp, OHAp) (Ref 38), it is not easy to distinguish them by XRD so it is necessary to use other techniques. The structural distortion and dehydroxylation state of the HAp in the coatings can be studied by means FTIR.

Figure 1, curves b and c, shows the FTIR spectra of as-sprayed and heat-treated HAp coatings, respectively. Table 1 summarizes the absorption bands observed in the spectra. The hydroxyl stretch band at 3572 cm^{-1} was observed in the spectra of the powder (Fig. 1, curve a) and for both coatings (Fig. 1, curves b and c). Furthermore, in the as-sprayed coating spectra, this hydroxyl band has a lower intensity compared to the feedstock powder and the heat-treated coating and there is no presence of the libration mode at 630 cm^{-1} of the hydroxyl vibration.

The presence of the characteristic OH vibration mode at 3572 cm^{-1} and the librational mode at 630 cm^{-1} coupled with the splitting of the major PO_4^{3-} absorption bands of the vibrational modes at 1090, 1048, 960, 601, and 570 cm^{-1} assured the presence of HAp in the coating after the heat treatment (Ref 39). There was no evidence, in the FTIR spectra, of CO_3^{2-} absorption (ν_3) that occurs as a broad doublet at about 1465 and 1412 cm^{-1} (Ref 40). Consequently, the heat treatment in an air atmosphere may produce a rehydroxylation of the coating.

3.6 Immersion Test

The surface morphology of the as-sprayed coating changes with the immersion time, while the heat-treated coating remains unchanged (Fig. 5 and 6, respectively). After 24-h immersion, the surface of the as-sprayed coating is completely covered with cauliflower-like precipitates and cracks were found along the whole surface (Fig. 5(b)). According to Li et al. this phenomenon is believed to be due to the enhanced bioactivity coupled with diffusion reactions between the coating surface and the SBF (Ref 41). Precipitates are present on the as-sprayed coating surface after 1 day of immersion. The quantity and size of the precipitation increase as the immersion time increases. These precipitates commonly appear in HAp coatings immersed in solutions containing Ca^{2+} cations and PO_4^{3-} anions and they were previously reported as apatite (Ref 42). There were no precipitates on the surface of the heat-treated coating after 7 days of immersion (Fig. 6).

The evolution of the Ca^{2+} and HPO_4^{2-} concentrations in the SBF after the immersion test, for as-sprayed coatings, is shown in Fig. 7. It can be seen how the concentrations decrease with time due to the precipitation of apatite onto the coating surface.

3.7 Bond Strength

The bond strength data were acquired following the ASTM F1147-99 designation. Each value reported is the average of three measurements. The results are summarized in Fig. 8. It was found that the tensile adhesion for the as-sprayed coating was 37.5 ± 4.8 MPa, whereas for heat-treated coating was 44.2 ± 8.3 MPa. The value

decreases to 14.5 and 9.16 MPa after 1 and 7 days of immersion for the as-sprayed coating. A change in the failure type was found. An adhesive-cohesive failure was found before immersion, while a completely adhesive failure was found after immersion. No deterioration of bond strength was observed after 7 days of immersion for heat-treated coating. The values ranged from 36.9 to 47.0 MPa.

4. Discussion

The most important issue in a cementless prosthesis is the quality of the coating which is considered to affect the coating resorption, bone in growth, and mechanical fixation of the implant. It had been suggested that the ideal HAp coating for orthopedic applications would be one with strong cohesive strength, good adhesion to the substrate, high chemical and phase stability and a high degree of crystallinity. Nowadays, the crystallinity degree is one of the main controversies in the HAp coated prosthesis. It is well-known that thermal spraying processes induce the presence of other calcium phosphates as TCP, TTCP, or CaO in the coating. Crystalline HAp is very stable in body fluids, but the dissolution rates of other calcium phosphates are higher than HAp and compromises the coating stability (Ref 43). On the other hand, these impurity phases with higher dissolution rate than HAp can accelerate the fixation of the implant and promote faster bone remodeling.

The phases detected in the as-sprayed coatings by x-ray diffraction were crystalline HAp, or OHA, and ACP. Due to the high temperatures achieved during thermal spraying processes the HAp feedstock particles are deposited in a molten or semimolten condition to form the coating. The spraying molten parts of the particles could undergo some dehydroxylation according to the reaction (1) (Ref 44):

$$2OH^-_{(s)} = O^{2-}_{(s)} + V_{(s)} + H_2O_{(g)}. \quad \text{(Eq 1)}$$

Thus the HAp crystalline phase consists of unmolten, or partially molten, particles and crystallized HAp particles form the melt. Moreover, some authors have suggested that the removal of structural water from the lattice of hydroxyapatite produces a solid solution of hydroxyapatite and oxyapatite or, alternatively, a combination of both (Ref 38). Some hydroxyl-deficient regions which do not form the amorphous phase can undergo crystallization to oxyapatite if the cooling rate is slower than a critical value of formation of the amorphous phase (Ref 45).

It is quite difficult to distinguish HAp from OHAp with a qualitative x-ray diffraction pattern. Deeper investigation was carried out by x-ray diffraction using Rietveld analysis and FTIR. It was observed that the (001) diffraction peaks of the coatings were shifted to lower angles suggesting that the *c*-axis of the unit cell of the HAp was longer in the as-sprayed coatings than in the feedstock powder. It was reported by other authors that the *c*-axis of the unit cell of the OHAp is slightly larger than HAp (Ref 45). The main proof of the presence of OHAp in the as-sprayed coating was the FTIR spectra, where no evidence of the libration mode at 630 cm^{-1} of the hydroxyl group was observed. Thus the crystalline phase in the as-sprayed coating is supposed to be a solid solution of oxyapatite, oxyhydroxyapatite or, alternatively, a combination of HAp and OHAp/OAp.

Amorphous materials are commonly obtained by rapid cooling from molten state. Fast cooling reduces the mobility of the atoms before they can pack into a more thermodynamically favorable crystalline state. Even though fast quenching is critical for the formation of ACP, it also depends on the complex structure of the hexagonal HAp unit cell. Vacancies located on hydroxyl sites strongly enforce the retention of the ACP. Some authors observed an increasing amorphicity in powders with a lower hydroxyl content (Ref 46). In consequence, it is difficult for the crystalline phase to form after the melting due to the quenching of the molten shell of the sprayed particles and to the removal of hydroxyl ions (Ref 47).

After the chemical etching of the as-sprayed coating, it was observed that the ACP phase was observed at the interface of every lamella, parallel to the interface substrate-coating and in the interface coating-substrate. A sprayed semimolten HAp particle can be understood as a three-shell structure. The outer shell of the sprayed particles is molten and dehydroxylated due to the heat, the intermediate layer is supposedly formed by a stoichiometric melt and the inner core is still solid and maintains the stoichiometry (Ref 48, 49). Once the sprayed particle arrives to the substrate the droplet spreads.

The coating is more amorphous at the interface substrate/coating than on the surface (Fig. 3(b)). The cooling rate of the first lamella was controlled by rapid heat dissipation to the metallic substrate. The dehydroxylated region near the substrate solidifies to ACP, but the area far away from the substrate crystallizes to form oxyapatite. Then, as consecutive layers are deposited, the cooling rate becomes much slower because the thermal conductivity of HAp [0.72-2.16 W/m·K (Ref 49-51)] is much lower than for Ti6Al4V. This results in more crystallization when the melt impacted onto previous deposited coating.

Amorphous calcium phosphate is a metastable phase and always tends to revert back to a more stable crystalline structure through a process of crystallization. Heat treatment at 700 °C for an hour accelerates the crystallization and leads to the increase of crystallinity of the Hap-sprayed coatings. The treatment was done in an air atmosphere furnace. It seems that atmospheric water molecules decrease the activation energy for the molecule diffusion and the free energy during the Hap crystal growth (Ref 52).

All ACP crystallized after the heat treatment giving a higher chemical stability against etching with the acidic solution (Fig. 5(b)). No evidence of amorphous phase was found. Furthermore, the *c*-axis length decreased and became more similar to that of the feedstock powder, so all the ACP was transformed to a solid solution of HAp, OHAp, or a combination of both.

The OHAp can transform to HAp by hydrolysis in order to decrease its free energy (Ref 40). The absorption

kinetics are mainly controlled by the partial pressure of water and the coating temperature. It is believed that residual stresses created during coating building up and structural imperfections in the coating can assist the transformation from oxyapatite to hydroxyapatite.

Scanning Electron Microscope observation showed the appearance of the coating surfaces were very similar before and after the heat treatment, so the crystallization do not affect the surface morphology. Cross section observation of the coatings show that porosity and cracks along the as-sprayed coating are reduced an hour after the heat treatment. The diffusion process that takes place at 700 °C will remove the cracks and pores on the coating with strong bonding between adjacent particles. The porosity influences the physical and mechanical characteristics of the coatings. A balance in the degree of porosity should be established since too high a porosity will affect the mechanical strength of the coating, but a porous structure also allows bone in growth, helping the implant fixation. Further in vitro and in vivo testing will provide information about how these coatings interact with the surrounding tissues.

Hydroxyapatite coatings behave differently in SBF depending on the heat treatment after spraying. Initially, amorphous (as-sprayed) coatings show a surface with tightly adhered splats with pores and cracks involved and small (>1 μm) unmolten particles (Fig. 6). The surface coating morphology changed after aging in Kokubo's solution for 1 day. Cracking is more intensive to the as-sprayed coating and an uniform layer of apatite was formed on the HAp coating after 14 days of immersion in Kokubo's SBF. Apatite nucleates and grows in cauliflower structure on amorphous coatings. It seems that this phenomenon indicates a higher bioactivity and an accelerated nucleation of the apatite on the HVOF-sprayed HAp coating. Due to instantaneous dissolution of ACP in the first hours, the concentrations of Ca^{2+} and HPO_4^{2-} increase to a maximum beyond their original concentrations in SBF after the immersion of the as-sprayed coatings. Once the solubility product of apatite has been reached and exceeded precipitation of secondary Ca-deficient defect apatite starts. This defect apatite in time tends to absorb Ca ions from the SBF. This effect was not observed for heat-treated coatings that do not contain enough ACP to establish a high concentration level of Ca^{2+} and HPO_4^{2-}.

It was seen that the adhesion strength in as-sprayed coating decreases considerably after aging in SBF, but the adhesion remains unchanged for the crystalline coatings. An adhesive-cohesive failure was found before immersion while a completely adhesive failure was found after immersion in as-sprayed coatings. Therefore, these results corroborate the evidence of the concentration of ACP on the interface substrate/coating of the as-sprayed coatings. The bond strength values are higher than those found in the literature for other thermal spraying techniques (Ref 53, 54). However, heat-treated coatings adhere better to the substrate due to the lack degradation in SBF and lower porosity, but show a low level of biomimetic activity to form secondary apatite on the surface in contact with SBF. A balance between the biomimetic activity of the as-sprayed coatings and the positive effect on the adhesive strength of the crystalline coatings should be taken into account. Both properties are desirable in a biocompatible coatings and efforts are moving in this direction.

5. Conclusion

- Hydroxyapatite coatings deposited by HVOF spraying show similar advantages as coatings obtained by APS, but with higher crystallinity: the as-sprayed coatings were found to contain only 18% of ACP. Since in accordance with Standard ISO 13779-2 (Ref 55) the crystalline content of HAp in a coating shall not be less than 45%, so HVOF is a promising method to obtain high crystalline HAp coatings.
- The amorphous phase concentrates at the interface substrate/coating due to the different temperatures between the substrate and the solidifying particles. It was also found at the interface of every lamella where the molten layer was formed during spraying.
- Heat treatment of the coating allows crystallization of the ACP present in the coatings. XRD analysis confirms that the ACP transforms directly to HAp and not to other calcium phosphate phases. Crystallization was also confirmed by chemical etching.
- Potential biomimetic activity was observed in as-sprayed coatings as calcium phosphate copiously precipitated at the coating surface after immersion in SBF. On the other hand, heat-treated coatings adhere better to the substrate due to the lack degradation of ACP in SBF and lower porosity, but show a low level of biomimetic activity to form secondary apatite on the surface in contact with SBF.
- The HVOF-sprayed HAp coating exhibited high bond strength. The bond strength decreases for the as-sprayed coatings after immersion in SBF, but it is constant for the heat-treated coatings. This phenomenon is related to the amorphous phase dissolution at the interface substrate-coating in as-sprayed coatings.

Acknowledgments

The authors want to thank the Generalitat de Catalunya for funding through the project 2001SGR00145 and the grant 2003FI 00384.

References

1. W. Suchanek and M. Yoshimura, Processing and Properties of Hydroxyapatite-based Biomaterials for Use as Hard Tissue Replacement Implants, *J. Mater. Res.*, 1998, **13**(1), p 94-117
2. K. Grootde, J.G.C Wolke, and J.A. Jansen, Calcium Phosphate Coatings or Medical Implants, *Proc. Inst. Mech. Eng. [H]*, 1998, **212**(2), p 137-147
3. R.G.T. Geesink, K. Grootde, and C.P.A.T. Klein, Chemical Implant Fixation using Hydroxylapatite Coatings. The Development of a Human Total Hip Prosthesis for Chemical Fixation to Bone

using Hydroxyl-apatite Coatings on Titanium Substrates, *Clin. Orthop. Rel. Res.*, 1987, **225**, p 147-170
4. C.A. Simmons, N. Valiquette, and R.M. Pilliar, Osseointegration of Sintered Porous-surfaced and Plasma spray-coated Implants: An Animal Model Study of Early Postimplantation Healing Response and Mechanical Stability, *J. Biomed. Mat. Res.*, 1999, **47**(2), p 127-138
5. G. Willmann, Coating of Implants with Hydroxyapatite-Material. Connections between Bone and Metal, *Adv. Eng. Mat.*, 1999, **1**(2), p 95-105
6. W.L. Jaffe and D.F. Scott, Total Hip Arthroplasty with Hydroxyapatite-Coated Hip Implants, *J. Bone Joint Surg. Am.*, 1996, **78**(12), p 1918-1934
7. W. Weng and J.L. Baptista, Alkoxide Route for Preparing Hydroxyapatite and its Coating, *Biomaterials*, 1998, **19**(1-3), p 125-131
8. D. Shi, G. Jiang, and J. Bauer, The Effect of Structural Characteristics on the In vitro Bioactivity of Hydroxyapatite, *J. Biomed. Res. Appl. Biomater.*, 2002, **63**(1), p 71-78
9. Y. Fu, A.W. Batchelor, and K.A. Khor, Fretting Wear Behavior of Thermal Sprayed Hydroxyapatite Coating Lubricated with Bovine Albumin, *Wear*, 1999, **230**(1), p 98-102
10. O.S. Yildirim, B. Aksakal, H. Celik, Y. Vangolu, and A. Okur, An Investigation of the Effects of Hydroxyapatite Coatings on the Fixation Strength of Cortical Screws, *Med. Eng. Phys.*, 2005, **27**(3), p 221-228
11. A.M. Ektessabi and M. Hamdi, Characterization of Calcium Phosphate Bioceramic Films using Ion Beam Analysis Techniques, *Surf. Coat. Technol.*, 2002, **153**(1), p 10-15
12. Y. Yang, K.H. Kim, and J.L. Ong, A Review on Calcium Phosphate Coatings Produced using a Sputtering Process-an Alternative to Plasma Spraying, *Biomaterials*, 2005, **26**(3), p 327-337
13. H.M. Kim, Ceramic Bioactivity and Related Biomimetic Strategy, *Curr. Opin. Sol. State Mat. Sci.*, 2003, **7**(4–5), p 289-299
14. S. Leeuwenburgh, P. Layrolle, F. Barrère, J. Bruijnde, J. Schoonman, C.A. Blitterswijkvan, and K. Grootde, Osteoclastic Resorption of Biomimetic Calcium Phosphate Coatings In vitro, *J. Biomed. Mater. Res.*, 2001, **56**(2), p 208-215
15. J. Fernández, M. Gaona, and J.M. Guilemany, Tribological Study of Plasma Hydroxyapatite Coatings. Bioceramics 16, *Key Eng. Mat.*, 2004, **254-256**, p 383-386
16. N. Aebli, J. Krebs, H. Stich, P. Schawalder, M. Walton, D. Schwenke, H. Gruner, B. Gasser, and J.C. Theis, In vivo Comparison of the Osseointegration of Vacuum Plasma Sprayed Titanium and Hydroxyapatite Coated Implants, *J. Biomed. Mater. Res: A*, 2003, **66A**(2), p 356-363
17. J. Fernández, J. M. Guilemany, and M. Gaona, High Crystallinity Degree Hydroxyapatite Coatings using HVOF Spraying, *Conference Proceedings ITSC*, E. Lugscheider, Ed., May 2-4, 2005, Basel, Switzerland (ISBN 3-87155-793-5) Ed., DVS/IIW/ASM-TSS, 2005, p 1219-1224
18. L. Sun, C.C. Berndt, K.A. Gross, and A. Kucuk, Material Fundamentals and Clinical Performance of Plasma-sprayed Hydroxyapatite Coatings: A Review, *J. Biomed. Mater. Res: Appl. Biomater.*, 2001, **58**(5), p 570-592
19. L. Sun, C.C. Berndt, K.A. Khor, H.N. Cheang, and K.A. Gross, Surface Characteristics and Dissolution Behavior of Plasma-sprayed Hydroxyapatite Coating, *J. Biomed. Mater. Res.*, 2002, **62**(2), p 228-236
20. P. Chean and K.A. Khor, Addressing Processing Problems Associated with Plasma Spraying of Hydroxyapatite Coatings, *Biomaterials*, 1996, **17**(5), p 537-544
21. V. V. Sobolev, J. M. Guilemany, and J. Nutting, *High Velocity Oxyfuel Spraying. Theory, Structure-Property Relationships and Applications*, Leeds (UK), Maney, 2004, p. 7-17, ISBN 1-902653-72-6
22. K.A. Khor, A. Vreeling, Z.L. Dong, and P. Cheang, Laser Treatment of Plasma Sprayed HA coating, *Mater. Sci. Eng. A.*, 1999, **266**(1), p 1-7
23. Y. Fu and A.W. Batchelor, Hot Isostatic Pressing of Hydroxyapatite Coating for Improved Fretting Wear Resistance, *J. Mat. Sci. Lett.*, 1998, **17**(20), p 1695-1696
24. Y.W. Gu, N.H. Loh, K.A. Khor, S.B. Tor, and P. Cheang, Spark Plasma Sintering of Hydroxyapatite, *Biomaterials*, 2002, **23**(1), p 37-43
25. C.F. Feng, K.A. Khor, S.W.K. Kweh, and P. Cheang, Thermally Induced Crystallization of Amorphous Calcium Phosphate in Plasma Spheroidised Hydroxyapatite Powders, *Mater. Lett.*, 2002, **46**(4), p 229-234
26. Z.E. Erkmen, The Effect of Heat Treatment on the Morphology of D-Gun Sprayed Hydroxyapatite Coatings, *J. Biomed. Mater. Res.: Appl. Biomater.*, 1999, **48**(6), p 861-868
27. H. Li, K.A. Khor, and P. Cheang, Properties of Heat-treated Calcium Phosphate Coatings Deposited by High-velocity Oxy-fuel (HVOF) Spray, *Biomaterials*, 2002, **23**(10), p 2105-2112
28. J.R. Davis, Ed., *Metals Handbook*, 9th ed. (Metals Park, Ohio), American Society for Metals, 1998, p 575-588, ISBN 0871706547 (prepared under the direction of the ASM International Handbook Committee)
29. R.M. Wilson, J.C. Elliott, and S.E.P Dowker, Rietveld Refinement of Crystallographic Structure of Human Dental Enamel Apatites, *Am. Miner.*, 1999, **84**, p 1406
30. T. Kokubo, H. Kushitani, and S. Sakka, Solutions Able to Reproduce In vivo Surface-structure Changes in Bioactive Glass-ceramic A-W3, *J. Biomed. Mater. Res.*, 1990, **24**(6), p 721-734
31. Standard Test Method for Tension Testing of Calcium Phosphate and Metal Coatings, F1147-01, ASTM Standards on disc, Philadelphia, Pa, ASTM, 2001
32. Card No. 9-432, Powder Diffraction File: Inorganic Phases, Joint Committee on Powder Diffraction Standards, Swarthmore, 1986
33. R.M. Wilson, J.C. Elliott, S.E.P. Dowker, and R.I. Smith, Rietveld Structure Refinement of Precipitated Carbonate Apatite using Neutron Diffraction Data, *Biomaterials*, 2004, **25**(11), p 2205-2213
34. T. Leventouri, Synthetic and Biological Hydroxyapatites: Crystal Structure Questions, *Biomaterials*, 2006, **27**(18), p 3339-3342
35. K. Nakamoto, *Infrared and Raman Spectra of Inorganic and Coordination Compounds* (New York), Wiley, 1986, ISBN 0-471-01066-9472–478
36. R.S. Lima, K.A. Khor, H. Li, P. Cheang, and B.R. Marple, HVOF Spraying of Nanostructured Hydroxyapatite for Biomedical Applications, *Mat. Sci. Eng. A*, 2005, **396**(1-2), p 181-187
37. H.C. Gledhill, I.G. Turner, and C. Doyle, Direct Morphological Comparison of Vacuum Plasma Sprayed and Detonation Gun Sprayed Hydroxyapatite Coatings for Orthopaedic Applications, *Biomaterials*, 1999, **20**(4), p 315-322
38. K.A. Gross, C.C. Berndt, R. Dinnebier, and P. Stephens, Oxyapatite in Hydroxyapatite Coatings, *J. Mater. Sci.*, 1998, **33**(15), p 3985-3991
39. I. Rehman and W. Bonfield, Characterization of Hydroxyapatite and Carbonated Apatite by Photo Acoustic FTIR Spectroscopy, *J. Mater. Sci: Mat. Med.*, 1997, **8**(1), p 1-4
40. J. C. Elliot. Structure and Chemistry of the Apatites and Other Calcium Orthophosphates, *Studies in Inorganic Chemistry*, J.C. Elliott, Ed., (Amsterdam), Elsevier, 1994 ISBN: 0-444-81582-1
41. J. Li, H. Liao, and M. Sjöström, Characterization of Calcium Phosphates Precipitated from Simulated Body Fluid of Different Buffering Capacities, *Biomaterials*, 1997, **18**(10), p 743-747
42. K. Hyakuna, T. Yamamuro, Y. Kotoura, M. Oka, T. Nakamura, T. Kokubo, and H. Kushitani, Surface Reactions of Calcium Phosphate Ceramics to Various Solutions, *J. Biomed. Mater. Res.*, 1990, **24**(4), p 471-478
43. S.R. Radin and P. Ducheyne, Plasma Spraying Induced Changes in Calcium Phosphate Ceramics and Effect on In vitro Stability, *J. Mater. Sci. Mater. Med.*, 1992, **3**(1), p 33-42
44. G. Montel, G. Bonel, J.-C. Trombe, J.-C. Heughebaert, and C. Rey, Progres dans le domaine de la chimie des composes phosphores solides a structure d'apatite. Application a la biologie et au traitement des minerais, *Pure Appl. Chem.*, 1980, **52**, p 973-987
45. K.A. Gross and C.C. Bernd, Thermal Processing of Hydroxyapatite for Coating Production, *J. Biomed. Mater. Res.*, 1998, **39**(4), p 580-587
46. J. Weng, X.G. Liu, X.D. Li, and X.D. Zhang, Intrinsic Factors of Apatite Influencing its Amorphization during Plasma-spray Coating, *Biomaterials*, 1995, **16**(1), p 39-44

47. K.A. Gross, C.C. Berndt, and H. Herman, Amorphous Phase Formation in Plasma-sprayed Hydroxyapatite Coatings, *J. Biomed. Mater. Res.*, 1998, **39**(3), p 407-414
48. K. A. Khor and P. Cheang, ''Characterization of Plasma-sprayed Hydroxyapatite Powders and Coatings,'' *Thermal Sprayed Coatings. Research, Design and Applications*, C.C. Berndt and T.F. Bernecki, Ed., ASM International, Anaheim, CA, 1993, p 347-352
49. S. Dyshlovenko, B. Pateyron, L. Pawlowski, and D. Murano, Corrigendum to ''Numerical Simulation of Hydroxyapatite Powder Behaviour in Plasma Jet'', [*Surf. Coat. Technol.* 2004, **179**, p 110–117] *Surf. Coat. Technol*, 2004, **187**, p 408-409
50. S. Maruno, K. Hayashi, Y. Sumi, Y.F. Wan, and H. Iwata, *CRC Handbook of Bioactive Ceramics*, 2nd ed. T. Yamamuro, L.L. Hench, and J. Wilson, Ed., CRC Press, Boca Raton, USA, 1991, p 187-193
51. L. Sun, C.C. Berndt, R.S. Lima, A. Kucuk, and K.A. Khor, Effects of Spraying Parameters on Phase Formation and Distribution in Plasma-Sprayed Hydroxyapatite Coatings, *International Thermal Spray Conference 2000. Thermal Spray: Surface Engineering via Applied Research*, C.C. Berndt, Ed., May 8-11, 2000 (Montréal, Québec, Canada), ASM International, 2000
52. J. Chen, W. Tong, Y. Cao, J. Feng, and X. Zhang, Effect of atmosphere on phase transformation in plasma-sprayed hydroxyapatite coatings during heat treatment, *J. Biomed. Mat. Res.*, 1997, **34**(1), p 15-20
53. Y.C. Tsui, C. Doyle, and T.W. Clyne, Plasma Sprayed Hydroxyapatite Coatings on Titanium Substrates Part 1: Mechanical Properties and Residual Stress Levels, *Biomaterials*, 1998, **19**(22), p 2015-2029
54. P.L. Silva, J.D. Santos, F.J. Monteiro, and J.C. Knowles, Adhesion and Microstructural Characterization of Plasma-sprayed Hydroxyapatite/glass ceramic Coatings onto Ti-6Al-4V, *Surf. Coat. Tech.*, 1998, **102**(3), p 191-196
55. ISO 13779-2 Implants for Surgery—Hydroxyapatite—Part 2: Coating of Hydroxyapatite, International Organization for Standardization